International Journal of Thermophysics, Vol. 25, No. 3, May 2004 (© 2004)

PVTx Measurements for a H_2O + Methanol Mixture in the Subcritical and Supercritical Regions

A. R. Bazaev,[1] I. M. Abdulagatov,[1−3] J. W. Magee,[2] E.A. Bazaev,[1] A. E. Ramazanova,[1] and A. A. Abdurashidova[1]

Received January 22, 2004

PVTx relationships for a H_2O + CH_3OH mixture (0.36 mole fraction of methanol) were measured in a range of temperatures from 373 to 673 K and pressures between 0.042 and 90.9 MPa. The density ranged from 37.76 to 559.03 kg · m^{-3}. Measurements were made with a constant-volume piezometer surrounded by a precision thermostat. The temperature inside the thermostat was maintained uniform within 5 mK. The volume of the piezometer (32.68 ± 0.01 cm^3) was previously calibrated from well-established *PVT* values of pure water (IAPWS), and was corrected for both temperature and pressure expansions. Uncertainties of the density, temperature, and pressure measurements are estimated to be 0.16%, 30 mK, and 0.05%, respectively. The uncertainty in composition is 0.001 mole fraction. The method of isochoric and isothermal break points was used to extract the phase transition temperatures, pressures, and densities for each measured isochore and isotherm. The values of the critical temperature, pressure, and density of the mixture were also determined from *PVTx* measurements in the critical region.

KEY WORDS: coexistence curve; constant-volume piezometer; critical point; methanol; supercritical mixture; vapor pressure; water.

1. INTRODUCTION

Supercritical fluids are attractive media for conducting chemical reactions because one can adjust the reaction environment (e.g., solvent properties)

[1] Institute for Geothermal Problems of the Dagestan Scientific Center of the Russian Academy of Sciences, Shamilya Str. 39-A, Makhachkala 367003, Dagestan, Russia.
[2] Physical and Chemical Properties Division, National Institute of Standards and Technology, 325 Broadway, Boulder, Colorado 80305–3328, U.S.A.
[3] To whom correspondence should be addressed. E-mail: ilmutdin@boulder.nist.gov

0195-928X/04/0500-0805/0

by manipulating temperature and pressure. Near the critical point, the properties of the solvent (water) are very sensitive to small changes in T and P. Water at supercritical conditions is a good medium for methane conversion to methanol, because this process occurs in the homogeneous gas phase at high pressures and at a temperature around 673 K [1, 2]. To understand and control this process, it is necessary to know thermodynamic, particularly $PVTx$, properties for H_2O + CH_3OH mixtures at near-critical and supercritical conditions. The use of supercritical water as a medium for methane conversion is an interesting proposition, because it provides a new approach to the problem of converting methane to high yields of oxygenates. The fundamental problem with existing catalytic and homogeneous gas-phase schemes is that the target products (methanol) are more reactive than methane, so conditions that promote methane conversion promote even more rapid degradation of the desired products. Incremental improvements in the existing schemes will not lead to the high yields required for commercial viability [3, 4]. Novel approaches are required to overcome this fundamental barrier. Supercritical technology might represent one such novel approach [1]. Methanol in water is also of interest for other technological processes [5, 6]. Webley and Tester [7] studied the fundamental kinetics of methanol oxidation in supercritical water in a temperature range from 723 to 823 K and at a pressure of 24.6 MPa.

Methanol is a structured, small and highly polar molecule and may be expected to interact strongly with other fluids in an H-bonded network [8]. Methanol molecules strongly affect, for example, water structure [9–12]; therefore, the H_2O + CH_3OH mixture shows anomalies in various physical properties. In mixtures containing methanol, the thermodynamic properties often exhibit anomalies. For example, the heat capacity for a small concentration of methanol (10 mol%) in water is shows a maximum [13–15]. The sound absorption in a H_2O + CH_3OH mixture decreases with an increase in temperature [16, 17]. Sound velocity and adiabatic compressibility in water + methanol mixtures [18] have a maximum and minimum with methanol concentration, respectively.

A new precise measurement of thermal ($PVTx$) or caloric ($C_V VTx$) properties is needed to study the effect of H-bonding on the structural and thermodynamic properties of H_2O + CH_3OH mixtures. These data can be useful also in developing physicochemical models of the thermodynamic properties of H-bonding mixtures such as H_2O + CH_3OH and to study the effect of supercritical media (supercritical water) on H-bonding.

2. LITERATURE REVIEW

Thermodynamic properties of H_2O + CH_3OH mixtures at near-critical and supercritical conditions are extremely scarce. Existing sources of thermodynamic properties of H_2O + CH_3OH mixtures in the sub- and supercritical regions exhibit significant differences in their overlapping regions. Most of the reported *PVTx* data [19–22] are at low temperatures (up to 420 K) in the liquid phase. Low-temperature and low-pressure *PVTx* measurements for H_2O + CH_3OH mixtures have been reviewed in our previous paper (Aliev et al. [23]). Therefore, some of the thermodynamic data at high temperatures (above 450 K) and high pressures recently reported are briefly reviewed here.

Xiao et al. [21] made density measurements of H_2O + CH_3OH mixtures relative to water in a vibrating-tube densimeter at temperatures up to 573 K and at pressures of 7 and 13.5 MPa. Excess molar volumes v_m^E were calculated from the experimental densities for the mixtures using accurate equations of state (IAPWS [24] for water and IUPAC [25] for methanol). Shahverdiyev and Safarov [26] reported *PVTx* results for H_2O + CH_3OH mixtures using a constant-volume piezometer. The temperature ranged from 298 to 523 K for compositions of 0.25, 0.5, and 0.75 mole fraction. The pressure ranged from bubble points up to 60 MPa. Griswold and Wong [27] measured the vapor-liquid *PTxy* relationship (bubble and dew points) of H_2O + CH_3OH mixtures along four isotherms (373, 423, 473, and 523) K using a pressure equilibrium still. The values of the critical pressure and critical temperature were determined from measured values of *PTx*.

Other thermodynamic properties such as the specific heat capacity at constant volume of a H_2O + CH_3OH mixture were reported by Polikhronidi et al. [28]. They measured the heat capacity at constant volume for an equimolar H_2O + CH_3OH mixture in the temperature range from 371 to 579 K and at densities between 245 and 395 $kg \cdot m^{-3}$. Measurements were made with a high-temperature, high-pressure, and nearly constant-volume calorimeter. These ranges included the liquid-vapor coexistence curve, and critical and supercritical conditions. The critical-temperature and the critical-density values were extracted from measured values of saturated densities near the critical point. The same apparatus was used to measure the isochoric heat capacity C_{VX} for a (0.5 mass fraction) H_2O + (0.5 mass fraction) CH_3OH mixture by Abdulagatov et al. [29] in the temperature range between 435 and 645 K and at densities from 250 to 450 kg m^{-3}.

Marshall and Jones [30] reported liquid-vapor critical temperatures for H_2O + CH_3OH mixtures over a wide range of composition, namely, 0.123, 0.232, 0.360, 0.511, and 0.755 mole fraction of methanol. For the

composition of the present study ($x = 0.36$ mole fraction of methanol), the measured value of the critical temperature by Marshall and Jones [30] is $T_c = 583.15$ K. Measurements were made with a visual method, where the value of the critical temperature is that at which the meniscus separating liquid and vapor phases disappears at equal volumes of the two phases. The critical temperature was measured with an estimated uncertainty of ± 0.4K. The uncertainty in the concentration is ± 0.5 mass%.

The possibility of chemical reactions during thermophysical property measurements for pure methanol was reported in several studies [31–36]. Measurements at high temperatures for pure methanol by Straty et al. [32], Ta'ani [33], and Bazaev et al. [36] showed a decomposition effect on *PVT* measurements. Analysis of the methanol sample after experiments showed the presence of hydrogen, carbon monoxide, carbon dioxide, formaldehyde, methyl formate, and dimethyl ether [31, 35, 36]. The presence of gases in liquid methanol after measurements has also been found in calorimetric experiments [29, 34]. But the possibility of methanol decomposition in near-critical and supercritical water and the effect of the supercritical media on H-bonding have not been studied previously. Therefore, the chromatographic analysis of the H_2O + CH_3OH samples after *PVTx* measurements in the near-critical and supercritical conditions are very important to check possible decomposition of the methanol molecules in supercritical water media.

The present paper reports the results of *PVTx* measurements, and derived dew-bubble pressures, saturated liquid and vapor densities for the H_2O + CH_3OH mixture ($x = 0.36$ mole fraction of methanol). Pressure vs temperature was measured along quasi-isochores. The data cover a density range from 37.76 to 559.03 $kg \cdot m^{-3}$ and a temperature range from 373 to 673 K. This range includes near-critical and supercritical conditions and the coexistence curve, and has extended the range of previous investigations.

3. EXPERIMENTAL PROCEDURE

The apparatus and procedures used for the *PVTx* measurements of the H_2O + CH_3OH mixture has been described in detail in previous papers [37–43]. Only essential information will be given here. The measurements were made using the constant-volume method. The high-pressure piezometer is constructed of heat- and corrosion-resistant high-strength alloy EI-43BU-VD (nickel—77.00%, chromium—19.84%, titanium—2.82%, aluminum—0.8%, iron—0.59%, silicon—0.44%, copper—0.01%). The inner volume of the piezometer was calculated by taking into consideration corrections for elastic pressure deformation and thermal expansion. The

inner volume of the piezometer was previously calibrated by filling it with distilled water and then withdrawing the water and weighing it. The mass of the water withdrawn $m(H_2O)$ yielded the volume of the piezometer $V_{T_0P_0} = m(H_2O)/\rho(H_2O)$ from the well-established density $\rho(H_2O)$ of water at temperature T_0 and pressure P_0 of the calibration. The density of water was calculated with a standard equation of state(EOS)(IAPWS, Wagner and Pruß [24]) at a temperature of $T_0 = 673.15$ K and a pressure of $P_0 = 38.40$ MPa. The uncertainty of the density calculation from the IAPWS formulation [24] at this condition is $\delta\rho_{H_2O} = 0.1\%$. All masses were determined with an uncertainty of 5×10^{-4} g or 0.003 to 0.04% (in this work we use a coverage factor $k = 2$). Therefore, in the worst case the volume of the piezometer at this temperature T_0 and pressure P_0 was determined with uncertainty of 0.14% ($\delta V_{P_0V_0} = \delta m + \delta\rho_{H_2O}$). The volume at these conditions, $V_{P_0,T_0} = (32.802 \pm 0.045)$ cm^3. This calibration was checked using other pure fluids. The resulting value of the piezometer volume was essentially the same as determined previously with water (difference is 0.12%).

It is necessary to know the volume of the piezometer, V_{PT}, at a given temperature T and pressure P for the purpose of calculating densities $\rho(T, P) = m/V_{PT}$. The effect of the temperature and pressure on the piezometer volume V_{PT} was estimated using the thermal expansion coefficient α of alloy EI-43BU-VD and the pressure expansion coefficient β of the piezometer. Variations of the piezometer volume V_{PT} with temperature T and pressure P were calculated with the equation [44],

$$V_{PT} = V_{P_0,T_0}[1 + 3\alpha(T - T_0) + \beta(P - P_0)], \tag{1}$$

where $\alpha = 1.56 \times 10^{-5}$ K^{-1} is the thermal expansion coefficient of the piezometer material, which is almost independent of temperature in the range from 370 to 700 K, and $\beta = 3.51 \times 10^{-5}$ MPa^{-1} is the pressure expansion coefficient of the piezometer. The values of α and β were determined also by using calibrations procedure with a standard fluid (pure water) between 373 and 675 K at pressures up to 100 MPa. The maximum uncertainty in the volume of the piezometer at a given temperature and pressure V_{PT} is related to the measured uncertainties of V_{P_0,T_0} (0.14%), the uncertainty of α and β, which was 10%, and uncertainties in pressure (0.05%) and temperature (0.0015%) as

$$\delta V_{PT} = \delta V_{P_0,T_0} + \frac{V_{P_0V_0}}{V_{PT}}\left[3\alpha[T - T_0)\delta\alpha + T\delta T] + \beta[(P - P_0)\delta\beta + P\delta P]\right]. \tag{2}$$

In the worst case (at a maximum pressure of 100 MPa and a maximum temperature of 673.15 K), the uncertainty in the V_{TP} determination

Table I. Experimental Pressure (in MPa) as a Function of Temperature and Density for $H_2O + CH_3OH$ Mixture ($x = 0.36$ mole fraction of methanol and ρ_{aver} = average density)

T (K)	P (MPa)	ρ (kg m^{-3})
$m = 1.2301$ g, $\rho_{aver} = 37.76$ kg · m^{-3}		
373.15	0.042	38.084
398.15	0.280	38.039
423.15	0.593	37.993
448.15	1.275	37.948
473.15	2.474	37.902
498.15	3.860	37.855
523.15	5.367	37.809
548.15	5.866	37.764
563.15	6.176	37.737
568.15	6.280	37.728
573.15	6.374	37.719
578.15	6.470	37.710
581.15	6.520	37.705
583.15	6.554	37.702
585.15	6.600	37.698
588.15	6.650	37.693
593.15	6.740	37.684
598.15	6.830	37.675
623.15	7.281	37.630
647.15	7.711	37.588
663.15	8.020	37.559
673.15	8.262	37.542
$m = 1.8277$ g, $\rho_{aver} = 56.10$ kg · m^{-3}		
373.15	0.068	56.583
398.15	0.322	56.516
423.15	0.623	56.449
448.15	1.326	56.381
473.15	2.531	56.313
498.15	3.928	56.244
523.15	5.726	56.175
548.15	7.601	56.105
563.15	8.152	56.065
568.15	8.320	56.051
573.15	8.492	56.038
578.15	8.630	56.024
581.15	8.730	56.016
583.15	8.842	56.011
585.15	8.850	56.006

Table I. *(Continued)*

T (K)	P (MPa)	ρ (kg m^{-3})
588.15	8.950	55.998
593.15	9.110	55.984
598.15	9.284	55.971
623.15	10.023	55.904
647.15	10.729	55.840
663.15	11.250	55.798
673.15	11.623	55.771
$m = 2.6784$ g, $\rho_{aver} = 82.21$ kg·m^{-3}		
373.15	0.096	82.919
398.15	0.372	82.821
423.15	0.663	82.722
448.15	1.393	82.623
473.15	2.598	82.523
498.15	4.047	82.422
523.15	6.005	82.320
548.15	8.501	82.216
563.15	9.952	82.154
568.15	10.310	82.134
573.15	10.650	82.114
578.15	10.862	82.094
581.15	11.080	82.082
583.15	11.139	82.074
585.15	11.280	82.066
588.15	11.440	82.054
593.15	11.653	82.034
598.15	11.970	82.014
623.15	13.174	81.915
647.15	14.245	81.821
663.15	14.952	81.758
673.15	15.456	81.718
$m = 2.7226$ g, $\rho_{aver} = 83.57$ kg·m^{-3}		
373.15	0.097	84.289
398.15	0.373	84.189
423.15	0.663	84.089
448.15	1.393	83.988
473.15	2.600	83.886
498.15	4.049	83.783
523.15	6.022	83.680
548.15	8.530	83.574
563.15	10.041	83.511
568.15	10.400	83.491
573.15	10.770	83.470

Table I. *(Continued)*

T (K)	P (MPa)	ρ (kg m^{-3})
578.15	10.980	83.450
581.15	11.170	83.438
583.15	11.250	83.430
585.15	11.370	83.422
588.15	11.540	83.409
593.15	11.810	83.389
598.15	12.060	83.369
623.15	13.347	83.268
647.15	14.504	83.172
663.15	15.240	83.108
673.15	15.714	83.068
$m = 4.1129$ g, $\rho_{aver} = 126.23$ kg·m^{-3}		
373.15	0.140	127.331
398.15	0.416	127.180
423.15	0.729	127.029
448.15	1.477	126.876
473.15	2.663	126.722
498.15	4.170	126.567
523.15	6.230	126.410
548.15	8.852	126.250
563.15	10.854	126.153
568.15	11.564	126.120
573.15	12.205	126.088
578.15	12.790	126.056
581.15	13.120	126.037
583.15	13.306	126.024
585.15	13.520	126.011
588.15	13.776	125.993
593.15	14.290	125.961
598.15	14.756	125.930
623.15	16.927	125.773
647.15	18.828	125.624
663.15	20.000	125.526
673.15	20.700	125.464
$m = 5.4724$ g, $\rho_{aver} = 167.95$ kg·m^{-3}		
373.15	0.180	169.419
398.15	0.453	169.218
423.15	0.783	169.017
448.15	1.552	168.813
473.15	2.709	168.608
498.15	4.271	168.401
523.15	6.334	168.192

Table I. *(Continued)*

T (K)	P (MPa)	ρ (kg m^{-3})
548.15	9.037	167.979
563.15	11.066	167.850
568.15	11.840	167.806
573.15	12.583	167.762
578.15	13.340	167.719
581.15	13.880	167.692
583.15	14.164	167.675
585.15	14.390	167.658
588.15	14.865	167.631
593.15	15.434	167.589
598.15	16.110	167.546
623.15	19.097	167.333
647.15	21.949	167.130
663.15	23.750	166.995
673.15	24.851	166.911
$m = 6.4004$ g, $\rho_{aver} = 196.43$ kg m^{-3}		
373.15	0.206	198.148
398.15	0.475	197.912
423.15	0.819	197.677
448.15	1.600	197.439
473.15	2.730	197.200
498.15	4.325	196.957
523.15	6.365	196.713
548.15	9.110	196.464
563.15	11.180	196.312
568.15	11.920	196.261
573.15	12.670	196.210
578.15	13.610	196.158
581.15	14.110	196.127
583.15	14.430	196.106
585.15	14.700	196.086
588.15	15.190	196.055
593.15	15.920	196.004
598.15	16.740	195.953
623.15	20.380	195.700
647.15	23.561	195.460
663.15	25.740	195.299
673.15	27.090	195.199
$m = 7.5000$ g, $\rho_{aver} = 230.17$ kg·m^{-3}		
373.15	0.230	232.191
398.15	0.501	231.916
423.15	0.858	231.640

Table I. *(Continued)*

T (K)	P (MPa)	ρ (kg m^{-3})
448.15	1.640	231.361
473.15	2.753	231.081
498.15	4.378	230.797
523.15	6.381	230.510
548.15	9.180	230.218
563.15	11.280	230.039
568.15	12.004	229.980
573.15	12.737	229.920
578.15	13.694	229.859
581.15	14.290	229.822
583.15	14.641	229.798
585.15	14.981	229.774
588.15	15.502	229.738
593.15	16.313	229.677
598.15	17.178	229.617
623.15	21.415	229.315
647.15	25.412	229.027
663.15	28.134	228.835
673.15	29.769	228.715
$m = 9.0626$ g, $\rho_{aver} = 278.12$ kg·m^{-3}		
373.15	0.266	280.567
398.15	0.533	280.233
423.15	0.907	279.900
448.15	1.700	279.563
473.15	2.780	279.225
498.15	4.423	278.881
523.15	6.391	278.535
548.15	9.280	278.181
563.15	11.440	277.965
568.15	12.120	277.894
573.15	12.875	277.821
578.15	13.755	277.748
581.15	14.360	277.703
583.15	14.745	277.674
585.15	15.200	277.643
588.15	15.686	277.600
593.15	16.680	277.525
598.15	17.748	277.450
623.15	22.801	277.078
647.15	27.634	276.722
663.15	30.970	276.484
673.15	33.028	276.335

Table I. *(Continued)*

T (K)	P (MPa)	ρ (kg m^{-3})
$m = 9.9832$ g, $\rho_{aver} = 306.37$ kg · m^{-3}		
373.15	0.282	309.066
398.15	0.553	308.699
423.15	0.935	308.332
448.15	1.728	307.961
473.15	2.793	307.588
498.15	4.440	307.210
523.15	6.407	306.829
548.15	9.350	306.438
563.15	11.510	306.200
568.15	12.210	306.121
573.15	12.930	306.042
578.15	13.850	305.961
581.15	14.470	305.911
583.15	14.880	305.878
585.15	15.290	305.845
588.15	15.820	305.797
593.15	16.800	305.715
598.15	17.878	305.632
623.15	23.662	305.214
647.15	29.170	304.815
663.15	32.930	304.548
673.15	35.259	304.382
$m = 10.4534$ g, $\rho_{aver} = 320.80$ kg · m^{-3}		
373.15	0.294	323.623
398.15	0.559	323.239
423.15	0.941	322.854
448.15	1.743	322.466
473.15	2.798	322.075
498.15	4.444	321.679
523.15	6.413	321.280
548.15	9.390	320.871
563.15	11.603	320.621
568.15	12.220	320.539
573.15	13.020	320.455
578.15	13.835	320.371
581.15	14.560	320.318
583.15	14.930	320.284
585.15	15.340	320.250
588.15	15.926	320.198
593.15	16.930	320.113
598.15	18.057	320.025
623.15	24.091	319.585

Table I. *(Continued)*

T (K)	P (MPa)	ρ (kg m^{-3})
647.15	29.925	319.163
663.15	33.934	318.881
673.15	36.370	318.706
$m = 10.8963$ g, $\rho_{aver} = 334.39$ kg·m^{-3}		
373.15	0.300	337.333
398.15	0.568	336.933
423.15	0.952	336.532
448.15	1.753	336.127
473.15	2.804	335.720
498.15	4.447	335.307
523.15	6.423	334.891
548.15	9.440	334.464
563.15	11.650	334.204
568.15	12.290	334.118
573.15	13.094	334.031
578.15	13.930	333.943
581.15	14.610	333.888
583.15	15.015	333.852
585.15	15.420	333.816
588.15	16.070	333.762
593.15	17.120	333.672
598.15	18.320	333.580
623.15	24.690	333.117
647.15	30.800	332.674
663.15	35.000	332.378
673.15	37.600	332.194
$m = 11.1241$ g, $\rho_{aver} = 341.38$ kg·m^{-3}		
373.15	0.304	344.387
398.15	0.572	343.978
423.15	0.960	343.569
448.15	1.757	343.156
473.15	2.808	342.740
498.15	4.449	342.319
523.15	6.430	341.894
548.15	9.460	341.458
563.15	11.680	341.192
568.15	12.290	341.105
573.15	13.124	341.015
578.15	13.970	340.925
581.15	14.660	340.869
583.15	15.045	340.833
585.15	15.500	340.796
588.15	16.090	340.741

Table I. *(Continued)*

T (K)	P (MPa)	ρ (kg m^{-3})
593.15	17.170	340.649
598.15	18.490	340.553
623.15	24.890	340.081
647.15	31.260	339.625
663.15	35.620	339.321
673.15	38.400	339.131
$m = 11.8256$ g, $\rho_{aver} = 362.90$ kg·m^{-3}		
373.15	0.313	366.103
398.15	0.582	365.668
423.15	0.971	365.233
448.15	1.763	364.793
473.15	2.817	364.352
498.15	4.460	363.904
523.15	6.449	363.452
548.15	9.500	362.988
563.15	11.720	362.705
568.15	12.370	362.612
573.15	13.194	362.517
578.15	14.100	362.421
581.15	14.790	362.362
583.15	15.250	362.322
585.15	15.700	362.282
588.15	16.320	362.224
593.15	17.580	362.123
598.15	18.900	362.022
623.15	25.740	361.514
647.15	32.830	361.021
663.15	37.551	360.693
673.15	40.533	360.488
$m = 12.1994$ g, $\rho_{aver} = 374.37$ kg·m^{-3}		
373.15	0.320	377.678
398.15	0.587	377.229
423.15	0.978	376.780
448.15	1.766	376.327
473.15	2.822	375.871
498.15	4.463	375.409
523.15	6.459	374.943
548.15	9.520	374.464
563.15	11.740	374.173
568.15	12.420	374.076
573.15	13.260	373.978
578.15	14.200	373.878
581.15	14.930	373.816

Table I. *(Continued)*

T (K)	P (MPa)	ρ (kg m^{-3})
583.15	15.395	373.775
585.15	15.840	373.735
588.15	16.590	373.673
593.15	17.850	373.569
598.15	19.190	373.464
623.15	26.400	372.935
647.15	34.008	372.420
663.15	38.900	372.079
673.15	41.874	371.868
$m = 13.3838$ g, $\rho_{aver} = 410.70$ kg·m^{-3}		
373.15	0.328	414.346
398.15	0.605	413.854
423.15	1.000	413.361
448.15	1.779	412.864
473.15	2.835	412.363
498.15	4.467	411.857
523.15	6.500	411.344
548.15	9.580	410.820
563.15	11.790	410.476
568.15	12.540	410.380
573.15	13.464	410.284
578.15	14.544	410.173
581.15	15.250	410.103
583.15	15.852	410.059
585.15	16.436	410.012
588.15	17.336	409.941
593.15	18.880	409.790
598.15	20.530	409.701
623.15	29.040	409.102
647.15	37.651	408.526
663.15	43.200	408.142
673.15	46.600	407.901
$m = 14.3553$ g, $\rho_{aver} = 440.50$ kg·m^{-3}		
373.15	0.336	444.419
398.15	0.617	443.891
423.15	1.007	443.363
448.15	1.776	442.830
473.15	2.847	442.293
498.15	4.472	441.749
523.15	6.530	441.200
548.15	9.640	440.636
563.15	11.850	440.293
568.15	12.650	440.178

Table I. *(Continued)*

T (K)	P (MPa)	ρ (kg m^{-3})
573.15	13.690	440.059
578.15	15.000	439.936
581.15	15.930	439.860
583.15	16.570	439.809
585.15	17.270	439.757
588.15	18.290	439.680
593.15	19.970	439.552
598.15	21.940	439.419
623.15	31.760	438.757
647.15	41.030	438.125
663.15	47.210	437.705
673.15	51.000	437.444
$m = 14.9446$ g, $\rho_{aver} = 458.57$ kg · m^{-3}		
373.15	0.340	462.662
398.15	0.624	462.112
423.15	1.013	461.562
448.15	1.790	461.007
473.15	2.854	460.449
498.15	4.475	459.883
523.15	6.560	459.311
548.15	9.670	458.723
563.15	11.920	458.366
568.15	12.934	458.242
573.15	14.040	458.117
578.15	15.570	457.986
581.15	16.660	457.904
583.15	17.430	457.849
585.15	18.160	457.795
588.15	19.190	457.714
593.15	21.140	457.576
598.15	23.420	457.433
623.15	33.800	456.735
647.15	44.000	456.062
663.15	50.500	455.620
673.15	54.600	455.343
$m = 15.6530$ g, $\rho_{aver} = 480.28$ kg · m^{-3}		
373.15	0.343	484.595
398.15	0.629	484.019
423.15	1.017	483.443
448.15	1.798	482.862
473.15	2.861	482.277
498.15	4.479	481.684

Table I. *(Continued)*

T (K)	P (MPa)	ρ (kg m^{-3})
523.15	6.570	481.085
548.15	9.720	480.469
563.15	12.090	480.092
568.15	13.410	479.958
573.15	14.890	479.821
578.15	16.510	479.682
581.15	18.160	479.587
583.15	19.000	479.528
585.15	19.800	479.470
588.15	20.920	479.384
593.15	23.340	479.231
598.15	25.770	479.079
623.15	36.800	478.337
647.15	48.500	477.608
663.15	56.100	477.126
673.15	60.950	476.824
$m = 16.2208$ g, $\rho_{aver} = 497.67$ kg·m^{-3}		
373.15	0.345	502.173
398.15	0.633	501.576
423.15	1.021	500.979
448.15	1.810	500.376
473.15	2.867	499.770
498.15	4.480	499.156
523.15	6.584	498.535
548.15	9.880	497.894
563.15	12.752	497.495
568.15	14.500	497.348
573.15	16.350	497.200
578.15	18.500	497.046
581.15	20.120	496.949
583.15	20.900	496.889
585.15	21.900	496.825
588.15	23.200	496.733
593.15	25.730	496.573
598.15	28.300	496.413
623.15	40.180	495.629
647.15	52.600	494.861
663.15	61.300	494.343
673.15	66.800	494.019
$m = 17.3456$ g, $\rho_{aver} = 532.10$ kg·m^{-3}		
373.15	0.347	536.995
398.15	0.636	536.357

Table I. *(Continued)*

T (K)	P (MPa)	ρ (kg m^{-3})
423.15	1.020	535.718
448.15	1.815	535.074
473.15	2.874	534.426
498.15	4.481	533.769
523.15	6.600	533.104
548.15	10.551	532.407
563.15	16.150	531.929
568.15	18.650	531.759
573.15	20.966	531.591
578.15	23.690	531.416
581.15	25.420	531.310
583.15	26.328	531.243
585.15	27.350	531.175
588.15	29.070	531.068
593.15	31.930	530.892
598.15	34.940	530.712
623.15	48.700	529.839
647.15	63.400	528.977
663.15	73.400	528.400
673.15	79.700	528.039
$m = 18.2261$ g, $\rho_{aver} = 559.03$ kg·m^{-3}		
373.15	0.350	564.254
398.15	0.640	563.584
423.15	1.019	562.913
448.15	1.830	562.235
473.15	2.882	561.555
498.15	4.482	560.865
523.15	6.615	560.166
548.15	11.222	559.421
563.15	19.700	558.862
568.15	22.800	558.671
573.15	25.582	558.486
578.15	28.700	558.295
581.15	30.720	558.177
583.15	31.756	558.105
585.15	32.800	558.033
588.15	34.800	557.915
593.15	37.840	557.726
598.15	41.272	557.529
623.15	56.900	556.576
647.15	73.000	555.644
663.15	84.000	555.018
673.15	90.900	554.628

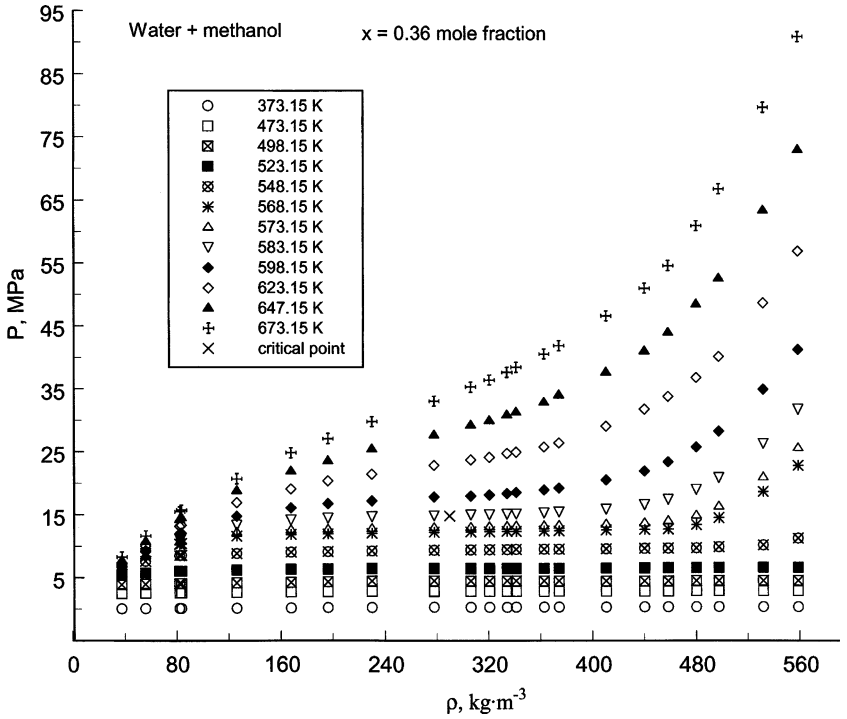

Fig. 1. Measured pressures P as a function of density ρ along various sub- and supercritical isotherms for a $(1-x)H_2O + xCH_3OH$ mixture in the single- and two-phase regions.

from Eq. (2) is 0.16%. Even if the values of α and β were determined with an uncertainty of 20%, the uncertainty in the V_{TP} determination is 0.18%. The pressure dependence of the piezometer volume ΔV_P was also calculated from the Lave formula [45] for the cylinder. The differences between experimentally determined values of ΔV_P and those calculated with the Lave formula are within 0.1%.

The fluid under study was thermostatted in a double-walled air bath. Stirring of the sample in the piezometer was accomplished with the aid of a steel ball inside the cell that was moved by oscillations of the thermostat with the piezometer. The fluid temperature was measured with a 10Ω platinum resistance thermometer (PRT-10). The PRT-10 was calibrated by VNIIFTRI (Moscow) with reference to the ITS-90. The maximum uncertainty in the measured temperature was 30 mK. The temperature inside the thermostat was maintained uniform within 5 mK with the aid

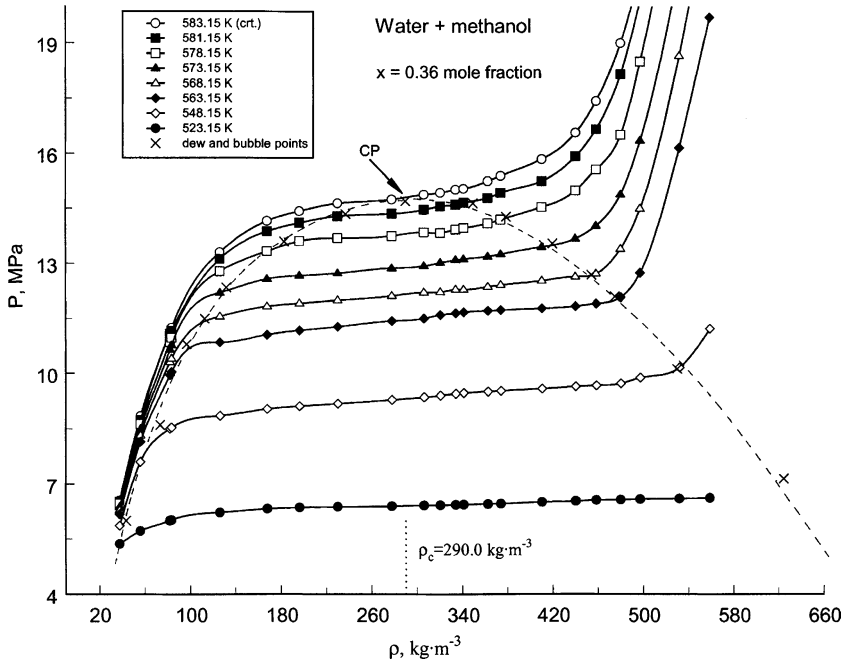

Fig. 2. Measured pressures P as a function of density ρ along various near-critical isotherms for a $(1-x)H_2O + xCH_3OH$ mixture. Solid curves are guides for the eye.

of guard heaters located between the thermostat walls and regulating heaters, which were mounted inside the thermostat. The temperature inside the thermostat and the fluid temperature were controlled automatically [46]. The thermostat has double walls with an inside volume of 65 dm^3. The heating elements were arranged between the walls. To minimize temperature gradients in the air thermostat, two electrically driven high-speed fans were used. The pressure in the piezometer was measured with an oil deadweight gauge with an estimated uncertainty of 0.05%.

The present experimental apparatus had no noxious ("dead") volumes [37–40]. Taking into account the uncertainties of measurements of temperature, pressure, and concentration, the total experimental uncertainty of density was estimated to be 0.163–0.20% ($\delta\rho = \delta V_{PT} + \delta m$) depending on the temperature and pressure. In order to check the reproducibility of the experimental values, some of the measurements at a selected temperature and pressure were repeated at different times. The reproducibility of the data corresponding to a repeated (P, T) point is better than $\pm 0.1\%$. To

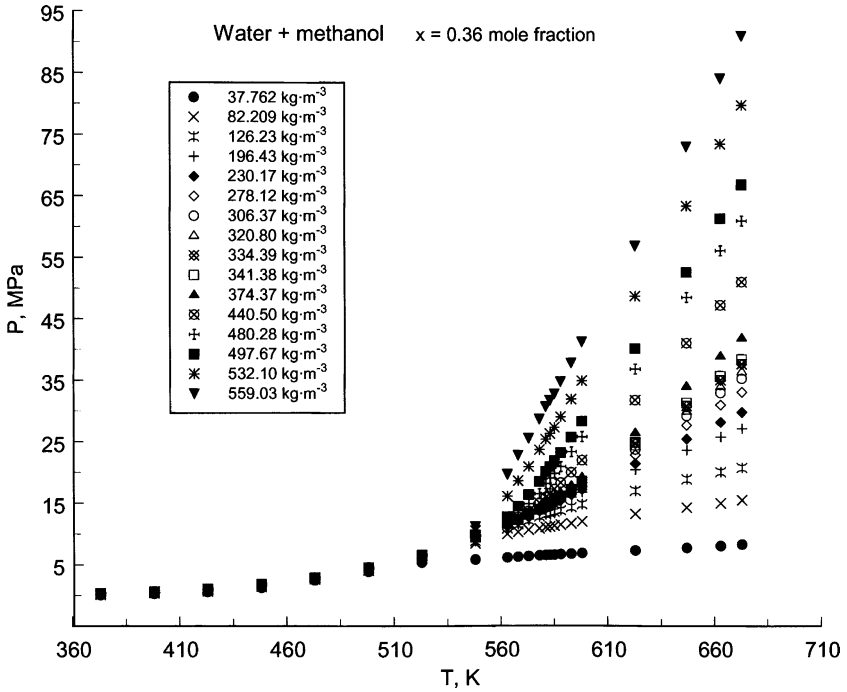

Fig. 3. Measured pressures P as a function of temperature T along various near-critical isochores for a $(1-x)H_2O + xCH_3OH$ mixture.

check and confirm the accuracy of the measurements, PVT measurements were made on pure water. The measured values of density and pressure for two supercritical isotherms, 653.15 and 673.15 K, of pure water were compared with data calculated from the IAPWS formulation [24] for pure water. The absolute average deviation between measured values of density and calculations with IAPWS [24] is AAD = 0.14% ($n = 20$). This agreement confirms the reliability and accuracy of the present PVT data for the $H_2O + CH_3OH$ mixture.

Pressure was measured as a function of density and temperature. The piezometer was filled at room temperature, sealed off, and heated along the quasi-isochore. After the cell reached the desired temperature, the sample was maintained in the piezometer for 2–3 h. After it reached equilibrium (pressure in the piezometer at a given temperature and density stabilized) at the desired temperature, the sample pressure was measured. After measurements, the sample was analyzed (by chromatograph Chrom-5) to check for decomposition. Analysis of the liquid phase

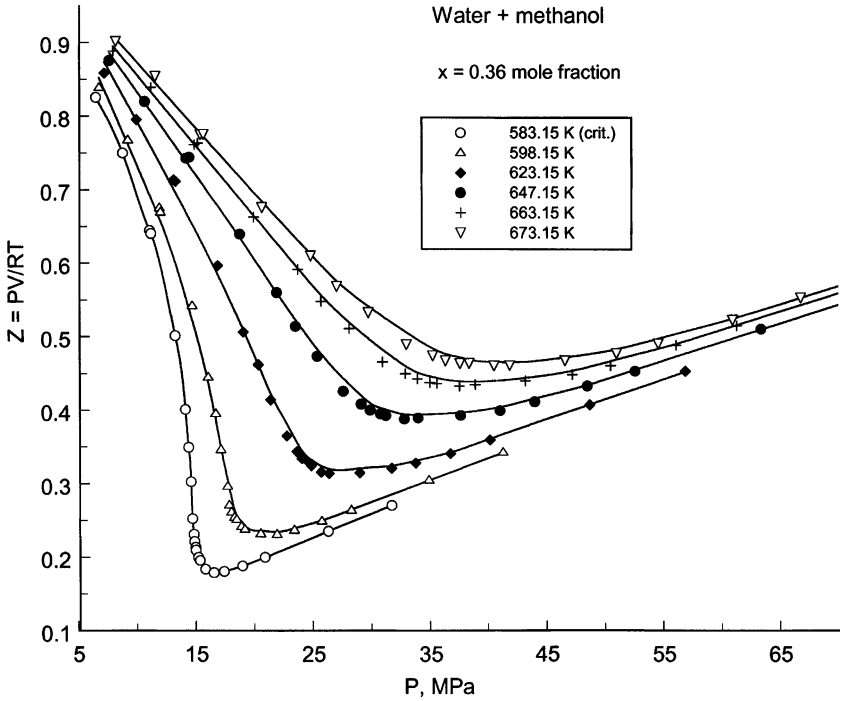

Fig. 4. Compressibility factor Z of a $(1-x)H_2O + xCH_3OH$ mixture as a function of pressure P in the vicinity of the critical point. Solid curves are guides for the eye.

showed the presence of formic acid (CH_2O)–0.04 mass% and dimethyl ether (CH_3OCH_3)–0.02 mass%. Therefore, in the presence of water, methanol molecules are more thermally stable compared with pure methanol at the same thermodynamic conditions [36]. After completion of the measurements for a given quasi-isochore, the piezometer was discharged and a new sample was used to continue the measurements for another quasi-isochore.

The commercial supplier of the methanol provided a purity analysis of 99.95 mol%.

4. RESULTS AND DISCUSSION

Measurements of *PVTx* properties for the aqueous methanol solution were performed along 22 isotherms between 373 and 673 K for one composition, $x = 0.36$ mole fraction of methanol. The pressure range was from 0.042 to 90.9 MPa. The experimental temperature, density, and pres-

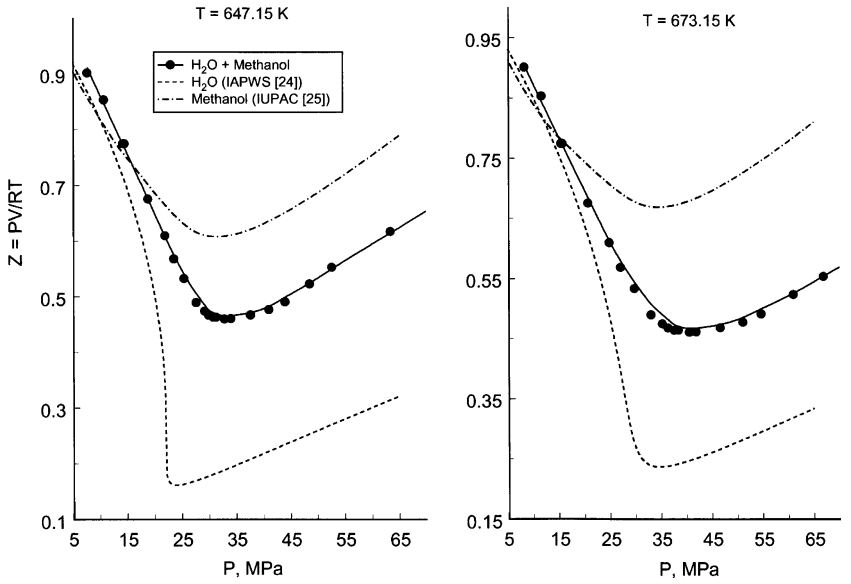

Fig. 5. Compressibility factor Z of $(1-x)H_2O + xCH_3OH$ mixture as a function of pressure P at near-critical (647.15 K) and supercritical (673.15 K) temperatures of pure water together with values calculated with IAPWS [24] and IUPAC [25] EOS for the pure components.

sure values are presented in Table I. Some selected experimental results are shown in Figs. 1–5 as projections in the P–ρ, P–T, and Z–P spaces. Figure 1 shows the density dependence of the pressure along various sub-critical and supercritical isotherms. The sub-critical isotherms included two- and single-phase measurements. The PVT behavior of the H_2O + CH_3OH mixture in the critical region is shown in Fig. 2, together with dew and bubble points for each measured isotherm derived graphically as discussed later in this section. The same data are depicted in Fig. 3 in a P–T diagram along various liquid and vapor isochores. The experimental compressibility factor $Z = PV/(RT)$ as a function of pressure P along the near-critical and supercritical isotherms is shown in Fig. 4. Figure 5 shows the values of the present experimental compressibility factor Z as a function of pressure P together with values calculated from IAPWS [24] and IUPAC [25] fundamental EOS for pure water and pure methanol, respectively, along the near-critical (647.15 K) and supercritical (673.15 K) isotherms of pure water. Figure 6 shows the experimental pressures of the H_2O + CH_3OH mixture ($x = 0.36$ mole fraction) as a function of density

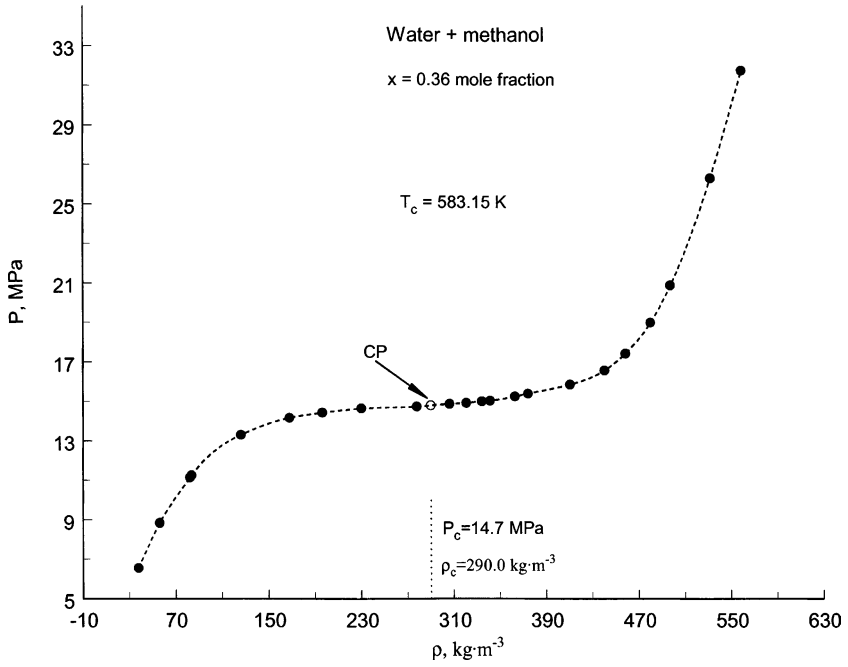

Fig. 6. Measured pressures P as a function of density ρ along the critical isotherm for $(1-x)H_2O + xCH_3OH$ mixture. Dashed curve is a guide for the eye.

along the critical isotherm (583.15 K) of mixture. Available experimental *PVTx* data [19–22] for H_2O + CH_3OH mixtures were measured at different concentrations, temperatures, and pressures, making it difficult to compare with our results. Only the data reported by Xiao et al. [21] for the isotherm of 573.6 K at a pressure of 13.7 MPa can be directly compared with present data. Figure 7 shows the results of such a comparison; the consistency between the measurements is good.

4.1. Determination of Phase Boundary Parameters (T_S, P_S, ρ_s', ρ_s'')

Figure 8a, b show examples of liquid and vapor single-phase and two-phase $P-\rho$ data along two selected sub-critical and near-critical isotherms 568.15 and 581.15 K. Each isotherm contains two break points, which correspond to the dew and bubble points. Between these break points (two-phase region), the $P-\rho$ dependence is almost linear. When approaching the critical isotherm (see Fig. 8a), it is increasingly difficult

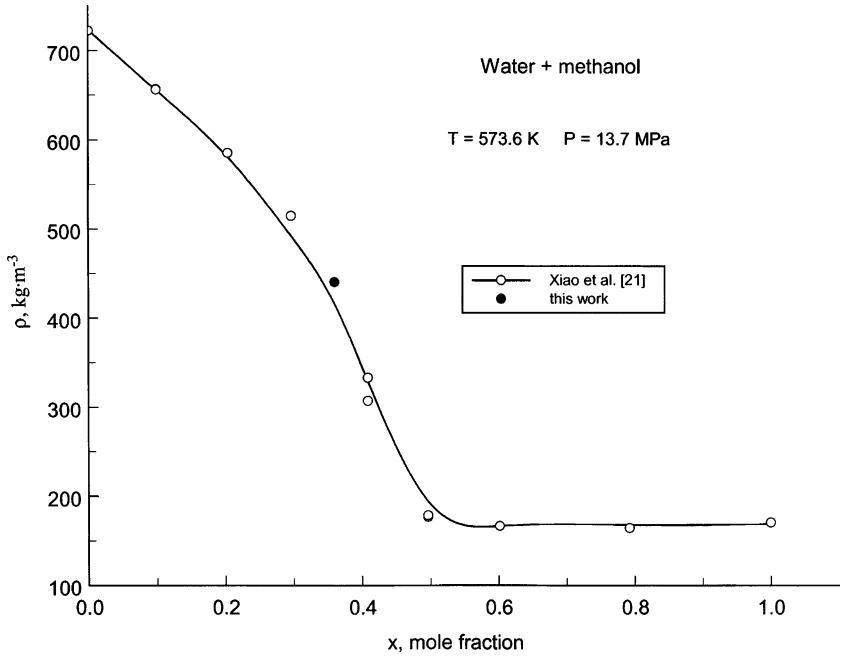

Fig. 7. Comparison of present experimental densities with the data reported by Xiao et al. [21] at 573.6 K and 13.7 MPa. Solid curve is a guide for the eye.

to differentiate between the single- and two-phase regions, while for the isotherms far from the critical region, break points are very clearly pronounced (see Fig. 8b). Near the critical point the transformation from the single- to two-phase (or from two- to single-phase) region take place without a sharp change (break) of the slope of the isotherm (continuously). Therefore, in the critical region, a phase transition determination by this method is considerably less accurate than far from the critical point where the slope of the isotherms changes sharply. For the critical region, a more suitable method would be the method of quasi-static thermograms which depends on the jump ΔC_V in heat capacity ($C_V \to \infty$ as $\Delta C_V \propto (T - T_C)^{-\alpha}$) when crossing any phase transition (calorimetric measurements [47–50]). The present experimental $PVTx$ data were used to extract the phase-boundary parameters (T_S, P_S, ρ'_S, ρ''_S) using a graphical technique for each measured sub-critical isotherm. Figure 9a, b shows the $P-T$ dependence along various selected liquid and vapor isochores. These figures show that the pressure after a phase transition (in the single-phase region) is almost a linear function of temperature. To extract the phase

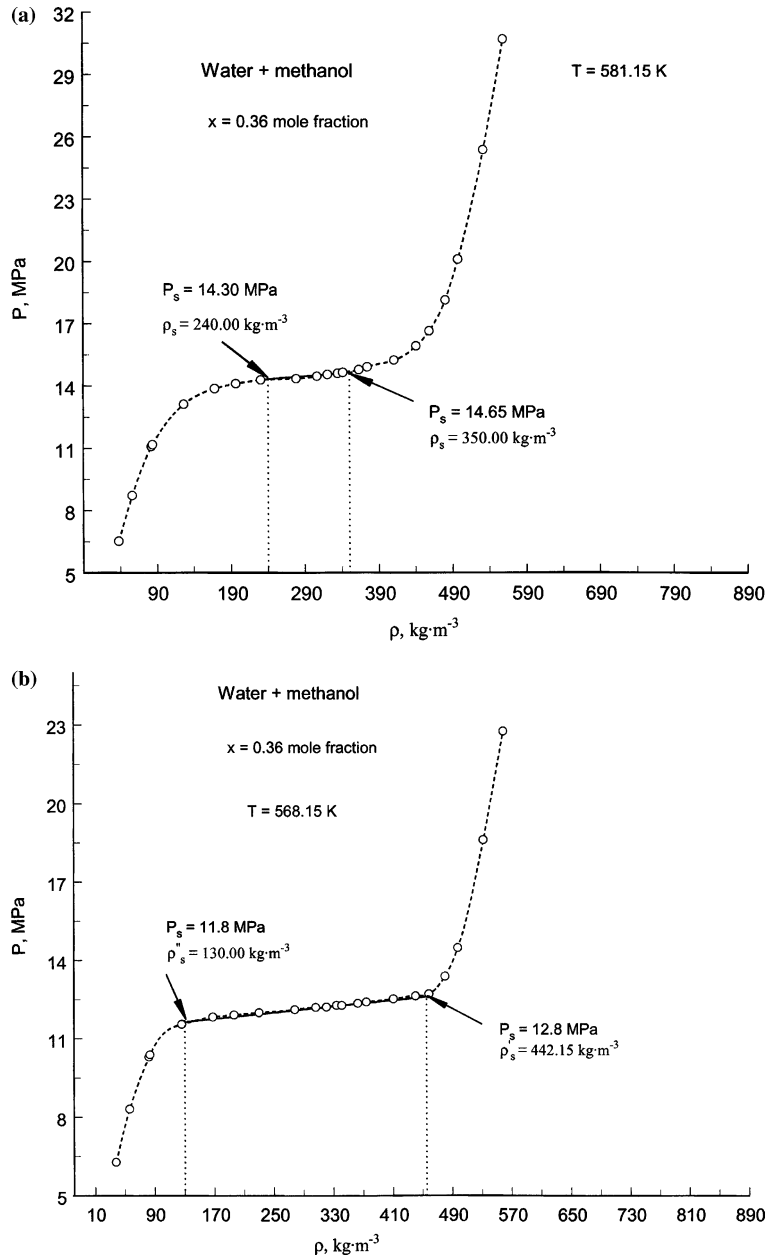

Fig. 8. Measured pressures P as a function of density ρ along two isotherms: (a) T=581.15 K and (b) 568.15 K, for $(1-x)H_2O + xCH_3OH$ mixture, showing isothermal break points. Dashed curves are guides for the eye.

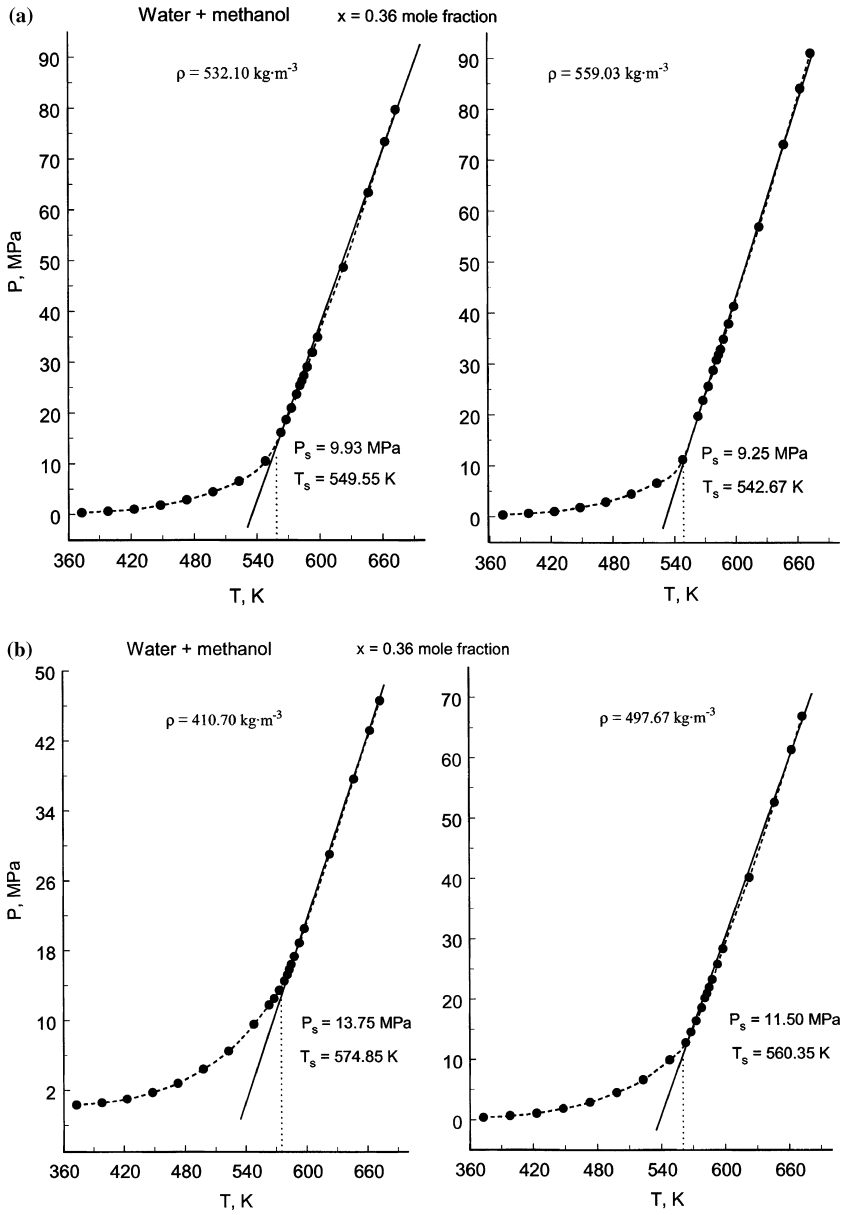

Fig. 9. Measured pressures P as a function of density ρ along various isochores: (a) $\rho = 532.10$ and 559.03 kg·m^{-3} and (b) $\rho = 410.70$ and 497.67 kg·m^{-3}, for $(1-x)H_2O + xCH_3OH$ mixture, showing isochoric break points. Dashed curves are guides for the eye.

transition temperature and the values of the pressure at this temperature, the initial points of the linear part of the $P-T$ curves were considered. The break points for the liquid isochores are seen very clearly; therefore, the accuracy of the extracted values of T_S and P_S for the liquid isochores is much better than for the near-critical isochores where the phase transition points show some spreading.

As one can see from Figs. 8a, b and 9a, b, each $P-\rho$ isotherm and $P-T$ isochore clearly exhibits the break points. The values of pressures P_S, densities ρ_S, and temperatures T_S at phase transition points (bubble and dew points) graphically extracted from the present experimental PVT data as isochoric and isothermal break points are given in Tables II and III. The average values of T_S and P_S have an uncertainty of about (0.2–0.5) K and (0.1–0.2) MPa in the range far from the critical point and (0.5–1.0) K and (0.3–0.5) MPa in the critical region, respectively. The uncertainty in saturated liquid and vapor densities is about 5 $kg \cdot m^{-3}$ in the range far from the critical point and is about 10 $kg \cdot m^{-3}$ in the critical region. The derived values of pressures P_S, densities ρ_S, and temperatures T_S at phase transition points (bubble and dew points) are plotted in Figs. 10 and 11, together with values reported in the literature. Figures 10 and 11 also include values of saturated densities and vapor pressures for the pure components calculated with the IAPWS [24] and IUPAC [25] EOS. Figure 10 also contains the saturated densities reported by other authors for the composition of 0.5 mole fraction. The experimental data and points calculated with the vapor-pressure correlation equation reported by Shahverdiyev and Safarov [26] for H_2O + CH_3OH mixtures ($x = 0.36$ mole fraction) are given in Fig. 11. The difference between the present results for bubble points and values calculated from correlation by Shahverdiyev and Safarov [26] is about 0.26% at high temperatures (473 K) and about 4% at low temperatures (323 K). Because the values of the phase transition temperatures T_S, pressures P_S, and densities were obtained by graphical methods as isochoric and isothermal break points, these data have relatively large uncertainties in comparisons with the methods of direct measurements.

4.2. Critical Parameters (P_C, ρ_C, T_C) Estimated from Near-Critical *PVTx* Measurements

There are no experimental data for the critical pressure and the critical density of this mixture. Isothermal liquid–vapor coexistence data were used by van Poolen and Holcomb [51] to estimate mixture critical parameters. The differences of the saturated liquid ρ'_S and vapor densities

Table II. Temperatures, Pressures, and Densities at Dew and Bubble Points from Isothermal Break Point Technique

T_S (K)	P_S (MPa)	ρ'_S (kg · m^{-3})	ρ''_S(kg · m^{-3})
523.15	7.14	624.7	43.7
5548.15	10.12	530.0	73.5
563.15	12.11	475.1	97.0
568.15	12.70	454.8	113.0
573.15	13.55	420.3	132.2
578.15	14.28	379.4	183.1
581.15	14.64	350.0	237.4
583.15	14.70	290.0	290.0

Table III. Temperatures, Pressures, and Densities at Bubble Points from Isochoric Break Point Technique

ρ_S (kg · m^{-3})	T_S (K)	P_S (MPa)
37.762	524.85	–
56.102	542.74	–
82.209	554.56	–
83.567	556.12	–
126.233	569.67	–
167.952	574.38	–
196.429	578.75	–
230.174	579.06	–
278.124	581.99	–
306.372	581.20	14.68
320.800	581.05	14.64
334.388	580.69	14.62
341.379	580.14	14.60
362.900	578.95	14.55
374.370	577.98	13.99
410.700	574.85	13.75
440.498	570.11	13.15
458.566	568.45	12.79
480.280	563.58	12.06
497.672	560.35	11.50
532.100	549.55	9.930
559.030	542.67	9.250

$\rho''_S(\Delta\rho = \rho'_S - \rho''_S)$ are fitted with an empirical function in $(P_C - P)/P_C$ to obtain the critical pressure, where P_C is an adjustable parameter. A scaling law analysis of $\Delta\rho$ vs. P data was used by Hsu et al. [52] to estimate the critical pressures for CO_2 + C_4H_8 mixtures. The technique used in

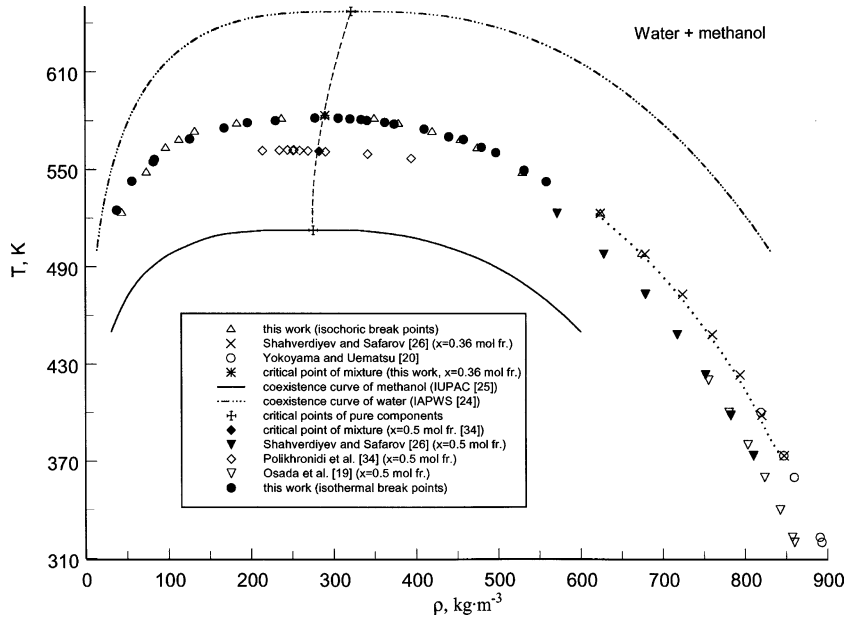

Fig. 10. Phase boundary in T–ρ plane derived from present *PVTx* measurements for $(1-x)H_2O + xCH_3OH$ mixture together with values reported in the literature and values for pure components calculated with IAPWS [24] and IUPAC [25] EOS.

this paper to estimate the critical parameters from derived phase boundary data is very close to the technique recommended by van Poolen and Holcomb [51] and Hsu et al. [52]. The pressure in the two-phase region between isothermal break points (dew and bubble points) is almost a linear function of density (see Fig. 8a, b). The width of the two-phase region ($\Delta\rho = \rho'_S - \rho''_S$) for each fixed isotherm approaches zero as the temperature approaches T_C. Figure 12 shows the pressure and temperature dependence of $\Delta\rho$ in the asymptotic region ($P \to P_C$). The values of the critical temperature and the critical pressure were determined by extrapolation of $\Delta\rho$ to zero. Our results are $T_C = 583.5 \pm 0.6$ K and $P_C = 15.0 \pm 0.4$ MPa. This value of the critical temperature is very close to the 583.15 K reported by Marshall and Jones [30] for same composition. The uncertainties in the critical parameter estimations depend on the uncertainty of the saturated densities (ρ'_S, ρ''_S) or $\Delta\rho$ to zero. Along the slightly sub-critical isotherm of 581.15 K, the width of the two-phase region is about $\Delta\rho = 110$ kg·m^{-3} ($\rho'_S = 350$ kg·m^{-3} and $\rho''_S = 240$ kg·m^{-3}). Therefore, the critical density

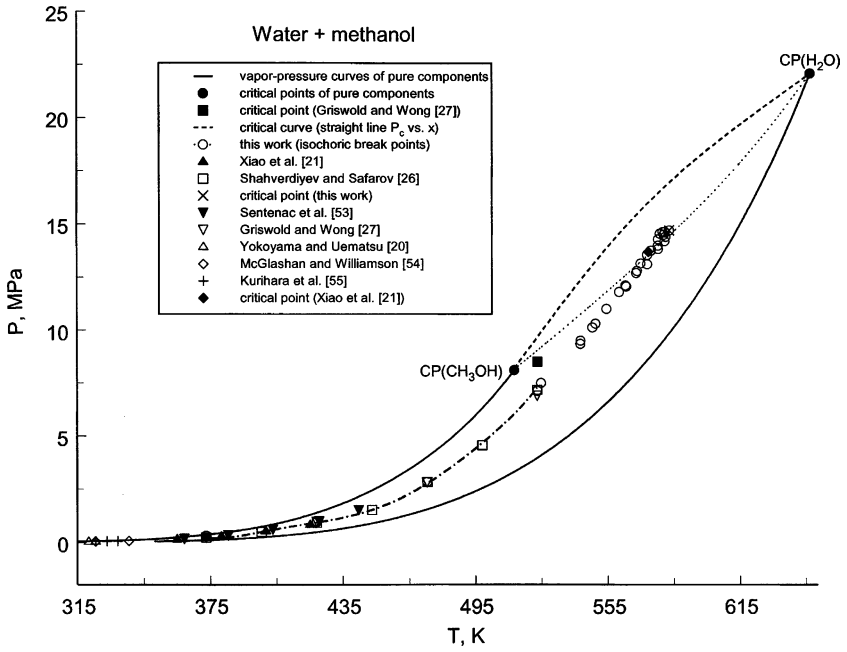

Fig. 11. Vapor-pressure and bubble curves for $(1 - x)H_2O + xCH_3OH$ mixture and pure components in the P–T plane derived from present $PVTx$ measurements using isothermal and isochoric break points together with values reported by other authors in the literature.

would lie between 240 and 350 kg m^{-3}. The most probable value of the critical density (the value of the density which correspond to the critical pressure of $P_C = 15.0$ MPa if it is assumed that the critical temperature is 583.15 K as reported by Marshall and Jones [30]) (see Fig. 6) is 290.0 ± 10 kg·m^{-3}. Our estimate of the uncertainty in the graphical determination of the critical pressure and the critical density determination is 0.4 MPa and 10 kg·m^{-3} or 2.0 and 3.4%, respectively. The values of the critical parameters (T_C, P_C, ρ_C) as a function of concentration (critical curves) for $H_2O + CH_3OH$ mixtures reported by various authors in the literature are given in Fig. 13a, b together with the present results. As these figures show, all reported data for the critical temperature, the critical pressure, and the critical density are consistent except for the data of Griswold and Wong [27]. The values of the critical temperature and the critical pressure reported by Griswold and Wong [27] are lower than the data by other authors.

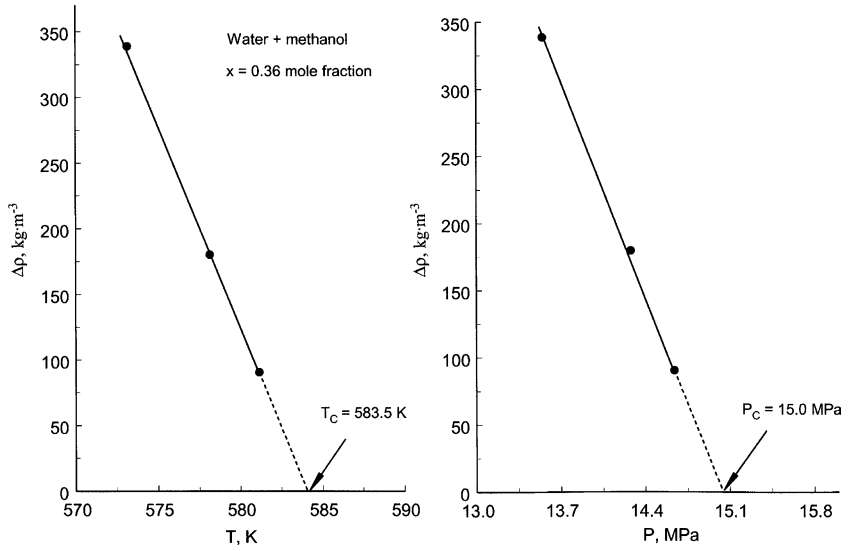

Fig. 12. $(\rho'_S - \rho''_S)$ versus P and T for $(1-x)H_2O + xCH_3OH$ mixture.

5. CONCLUSIONS

PVTx data for a H_2O + CH_3OH mixture ($x = 0.36$ mole fraction of methanol) are reported in a range of temperatures from 373 to 673 K and pressures between 0.042 and 90.9 MPa. The density ranged from 37.76 to 559 $kg \cdot m^{-3}$. Measurements were made with a constant-volume piezometer surrounded by a precision thermostat. Uncertainties of the density, temperature, pressure, and concentration measurements are estimated to be 0.16%, 30 mK, 0.05%, and 0.001 mole fraction, with a coverage factor $k = 2$, respectively. The method of isochoric and isothermal break points was used to extract the phase-transition temperatures and pressures for each measured isochore and isotherm. The values of the critical parameters (T_C, P_C, ρ_C) were determined using measured values of *PVTx* near the critical point.

ACKNOWLEDGMENTS

I. M. Abdulagatov thanks the Physical and Chemical Properties Division at the National Institute of Standards and Technology for the opportunity to work as a Guest Researcher at NIST during the course of this research. This work was also supported by the Grant of RFBR 03–02–16220.

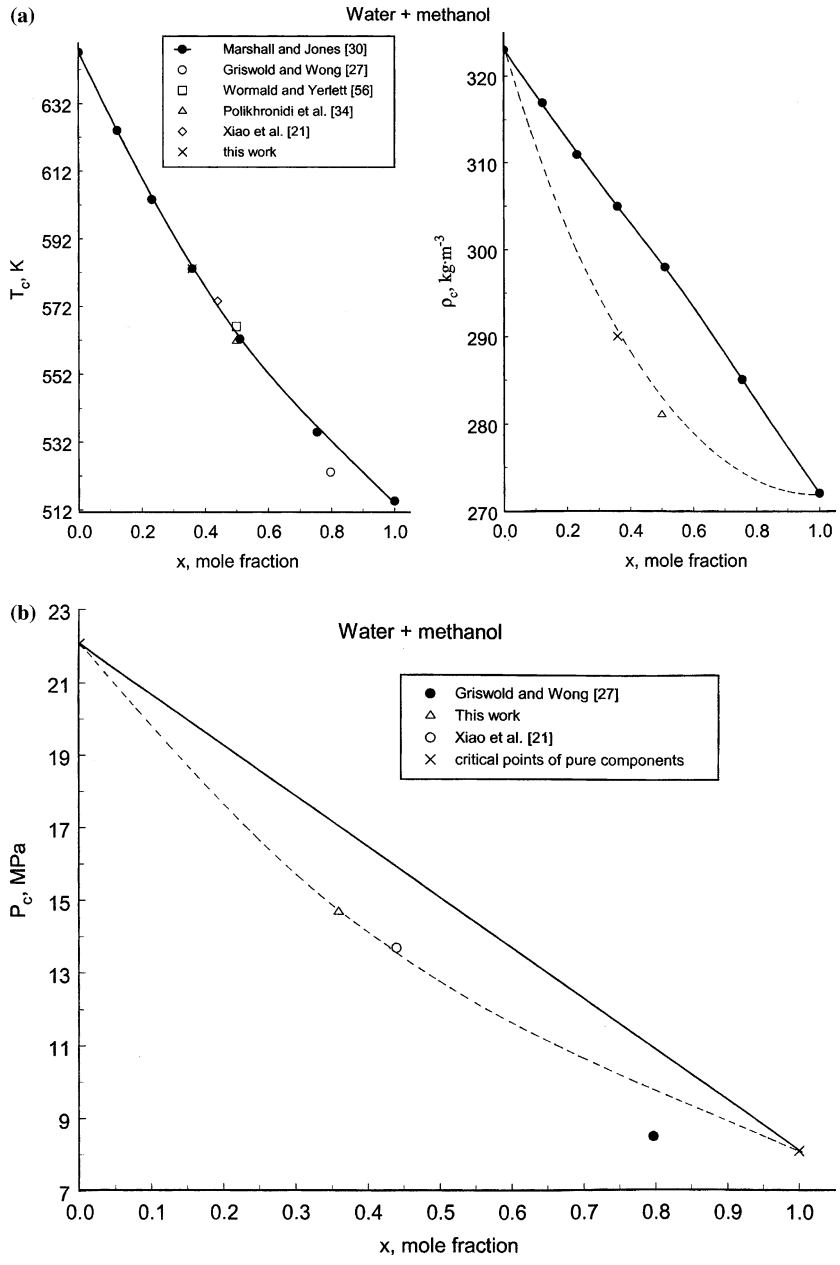

Fig. 13. Experimental critical lines: (a) T_c and ρ_c and (b) P_c, for $(1-x)H_2O + xCH_3OH$ mixtures. Solid and dashed curves are guides for the eye.

REFERENCES

1. P. E. Savage, R. Li, and J. T. Santini, *J. Supercrit. Fluids* **7**:135 (1994).
2. C. N. Dixon and M. A. Abraham, *J. Supercrit. Fluids* **5**:269 (1992).
3. J. A. Labinger, *ACS Div. Pet. Chem. Prepr.* 289 (1992).
4. R. A. Periana, D. J. Taube, E. R. Evitt, D. Loffler, P. R. Wentrcek, G. Voss, and T. Masuda, *Science* **259**:340 (1993).
5. S. Blanco, I. Velasco, E. Rauzy, and S. Otin, *J. Chem. Eng. Jpn.* **34**:971 (2001).
6. J. Liu, Z. Qin, and J. Wang, *Ind. Eng. Chem. Res.* **40**:3801 (2001).
7. P. A. Webley and J. W. Tester, *Supercritical Fluid Science and Technology* (ACS, Washington DC, 1989), Chap.17, pp. 259–275.
8. J. M. Simonson, D. J. Bradley, and R. H. Busey, *J. Chem. Thermodyn.* **19**:479 (1987).
9. Y. Marcus, *Phys. Chem. Chem. Phys.* **1**:2975 (1999).
10. A. Staib, *J. Chem. Phys.* **108**:4554 (1998).
11. G. Kabisch and K. Pollmer, *J. Mol. Struct.* **81:**35 (1982).
12. A. Laaksonen, P. G. Kusalik, and I. M. Svishchev, *J. Phys. Chem.* **A101:**5910 (1997).
13. R. Nakayama and K. Shinoda, *J. Chem. Thermodyn.* **3:**401 (1971).
14. V. P. Belousov and M. Yu. Panov, *Thermodynamics of the Nonelectrolyte Aqueous Solutions.* (Chemistry, Leningrad, 1983).
15. S. Yu. Noskov, M. G. Kiselev, and A. M. Kolker, *Russ. J. Struct. Chem.* **40:**40 (1999).
16. W. D. T. Dale, P. A. Flavell, and P. Kurrus, *Can. J. Chem.* **54:**355 (1976).
17. H. Endo, K. Saijou, and G. Atkinson, *J. Acoust. Soc. Jpn.* **13:**85 (1992).
18. I. Larionov, *Ph. D. thesis*, MPPI, Moscow, (1951).
19. O. Osada, M. Sao, and M. Uematsu, *J. Chem. Thermodyn.* **31:**451 (1999).
20. H. Yokoyama and M. Uematsu, *J. Chem. Thermodyn.* **35:**813 (2003).
21. C. Xiao, H. Bianchi, and P. R. Tremaine, *J. Chem. Thermodyn.* **29:**261 (1997).
22. A. A. Aliev, Ph.D. thesis, Institute of Physics of the Azerbadjan Academy of Sciences, Baku, (1988).
23. M. M. Aliev, J. W. Magee, and I. M. Abdulagatov, *Int. J. Thermophys.* **24:**1551 (2003).
24. W. Wagner and A. Pruß, *J. Phys. Chem. Ref. Data* **31:**387 (2002).
25. K. M. de Reuck and R. J. B. Craven, *International Thermodynamic Tables of the Fluid State-12. Methanol* (Blackwell Scientific, London, 1993).
26. A. N. Shahverdiyev and J. T. Safarov, *Phys. Chem. Chem. Phys.* **4:**979 (2002).
27. J. Griswold and S. Y. Wong, *Chem. Eng. Prog. Symp. Ser.* **48:**18 (1952).
28. N. G. Polikhronidi, I. M. Abdulagatov, J. W. Magee, and G. V. Stepanov, in preparation.
29. I. M. Abdulagatov, V. I. Dvoryanchikov, M. M. Aliev, and A. N. Kamalov, in *Steam, Water, and Hydrothermal Systems, Proc. 13th Int. Conf. on Props. of Water and Steam*, P. R. Tremaine, P. G. Hill, D. E. Irish, and P. V. Balakrishnan, eds. (NRC Research Press, Ottawa, 2000), p. 157.
30. W. L. Marshall and E. V. Jones, *J. Inorg. Nucl. Chem.* **36:**2319 (1974).
31. T. K.Yerlett and C. J. Wormald, *J. Chem. Thermodyn.* **18:**719 (1986).
32. G. C. Straty, A. M. F. Palavra and T. J. Bruno, *Int. J. Thermophys*. **7:**1077 (1986).
33. R. Ta'ani, Dr. Ing. thesis, Karlsruhe University (1976).
34. N. G. Polikhronidi, I. M. Abdulagatov, J. W. Magee, and G. V. Stepanov, *Int. J. Thermophys.*, in preparation.
35. T. J. Bruno and G. C. Straty, *J. Res. NBS* **91:**135 (1986).
36. A. R. Bazaev, I. M. Abdulagatov, J. W. Magee, E. A. Bazaev, and A. E. Ramazanova, *Int. J. Thermophys.*, in preparation.
37. I. M. Abdulagatov, A. R. Bazaev, and A. E. Ramazanova, *Int. J. Thermophys.* **14:**231 (1993).

38. A. R. Bazaev, I. M. Abdulagatov, J. W. Magee, E. A. Bazaev, and A. E. Ramazanova, *J. Supercritical Fluids* **26:**115 (2003).
39. I. M. Abdulagatov, A. R. Bazaev, E. A. Bazaev, M. B. Saidakhmedova, and A. E. Ramazanova, *Fluid Phase Equilibr.* **150:**537 (1998).
40. I. M. Abdulagatov, E. A. Bazaev, A. R. Bazaev, and M. G. Rabezkii, *J. Supercrit. Fluids* **19:**219 (2001).
41. M. G. Rabezkii, A. R. Bazaev, I. M. Abdulagatov, J. W. Magee, and E. A. Bazaev, *J. Chem. Eng. Data* **46:**1610 (2001).
42. A. R. Bazaev, I. M. Abdulagatov, J. W. Magee, E. A. Bazaev, and M. G. Rabezkii, *J. Chem. Eng. Data* **46:**1089 (2001).
43. S. B. Kiselev, J. F. Ely, I. M. Abdulagatov, A. R. Bazaev, and J. W. Magee, *Ind. Eng. Chem. Res.* **41:**1000 (2002).
44. D. S. Tsiklis, L. R. Linshiz, and I. B. Rodnina, *Thermophys. Properties Substances Mater.* **2:**268 (1969).
45. F. G. Keyes and L. B. Smith, *Proc. Am. Acad. Arts Sci.* **68:**505 (1933).
46. A. R. Bazaev, *Heat Transfer* **1:**113 (1988).
47. N. G. Polikhronidi, I. M. Abdulagatov, J. W. Magee, and R. G. Batyrova, *J. Chem. Eng. Data* **46:**1064 (2001).
48. N. G. Polikhronidi, I. M. Abdulagatov, J. W. Magee, and G. V. Stepanov, *Int. J. Thermophys.* **22:**189 (2001).
49. N. G. Polikhronidi, I. M. Abdulagatov, J. W. Magee, and G. V. Stepanov, *Int. J. Thermophys.* **23:**745 (2002).
50. N. G. Polikhronidi, I. M. Abdulagatov, J. W. Magee, and G. V. Stepanov, *Int. J. Thermophys.* **24:**405 (2003).
51. L. J. Von Poolen and C. D. Holcomb, *Fluid Phase Equilibr.* **165:**157 (1999).
52. J. J.-C. Hsu, N. Nagarajan, and R. L. Robinson, *J. Chem. Eng. Data* **30:**485 (1985).
53. P. Sentenac, Y. Bur, E. Rauzy, and C. Berro, *J. Chem. Eng. Data* **43:**592 (1998).
54. M. L. McGlashan and A. G. Williamson, *J. Chem. Eng. Data* **21:**196 (1976).
55. K. Kurihara, T. Minoura, K. Takeda, and K. Kojima, *J. Chem. Eng. Data* **40:**679 (1995).
56. C. J. Wormald and T. K. Yerlett, *J. Chem. Thermodyn.* **32:**97 (2000).